

Properties and alignment of interstellar dust grains toward Type Ia Supernovae with anomalous polarization curves

Thiem Hoang^{1, 2*}

¹ *Institute of Theoretical Physics, Goethe Universität Frankfurt, D-60438 Frankfurt am Main, Germany*

² *Current address: Canadian Institute for Theoretical Astrophysics, University of Toronto, 60 St. George Street, Toronto, ON M5S 3H8, Canada*

30 January 2019

ABSTRACT

Recent photometric and polarimetric observations of type Ia supernovae (SNe Ia) show unusually low total-to-selective extinction ratio ($R_V < 2$) and wavelength of maximum polarization ($\lambda_{\text{max}} < 0.4 \mu\text{m}$) for several SNe Ia, which indicates peculiar properties of interstellar (IS) dust in the SN hosted galaxies and/or the presence of circumstellar (CS) dust. In this paper, we use inversion technique to infer best-fit grain size distribution and alignment function of interstellar grains along the lines of sight toward four SNe Ia with anomalous extinction and polarization data (SNe 1986G, 2006X, 2008fp, and 2014J). We find that to reproduce low values of R_V , a significant enhancement in the mass of small grains of radius $a < 0.1 \mu\text{m}$ is required. For SN 2014J, a simultaneous fit to observed extinction and polarization data is unsuccessful if the entire data is attributed to IS dust (model 1), but a good fit is obtained when accounting for the contribution of CS dust (model 2). For SN 2008fp, our fitting results for model 1 show that, to reproduce an extreme value of $\lambda_{\text{max}} \sim 0.15 \mu\text{m}$, very small silicate grains must be aligned as efficiently as big grains. We suggest that tiny grains in the intervening molecular cloud can be aligned efficiently by radiative torques (RATs) from the SNe Ia. The resulting time dependence polarization from this RAT alignment model can be tested by observing at ultraviolet wavelengths. Our results are in favor of the existence of CS dust in SN 2014J, but its presence in SN 2008fp remains uncertain.

Key words: supernovae: general, supernovae: individuals (SNe 1986G, 2006X, 2008fp, 2014J), polarization- dust, extinction

1 INTRODUCTION

Type Ia supernovae (SNe Ia) have been used as standard candles to measure the expansion of the universe due to their stable intrinsic luminosity (Riess et al. 1998). Recently, a new avenue appears in using SNe Ia to study properties of dust in the interstellar medium (ISM) of distant galaxies (Nobili & Goobar 2008; Foley et al. 2014; Brown et al. 2014). This advancement is based on the strong dependence of peak luminosity on the reddening of SNe Ia by dust extinction (see Phillips et al. 2013).

Photometric observations of SNe Ia demonstrate peculiar dust properties with unprecedented low visual-to-selective extinction ratio $R_V = A_V/E_{B-V}$ where A_V is the optical extinction and E_{B-V} is the color excess. For instance, using data from 80 SNe Ia with considerable reddening (i.e., $E_{B-V} < 0.87$ mag), Nobili & Goobar (2008) report an unusually low value of $R_V \sim 1.75$ (see also Phillips et al.

2013), much lower than the typical value $R_V \sim 3.1$ for interstellar grains in the Milky Way. Recently, using data from UV to near-IR ($\lambda \sim 0.2 - 2 \mu\text{m}$) from Hubble and Swift satellites, Amanullah et al. (2015) present a diversity in extinction curves, with R_V ranging from 1.4 to 3 (see also Wang et al. (2012)). Unprecedented low values of R_V toward numerous SNe Ia are attributed to the scattering by circumstellar dust (hereafter CS dust; see, e.g. Goobar 2008). Numerous authors, however, suggest that the low values of R_V are due to the enhancement in the relative abundance of small grains of interstellar dust (hereafter IS dust) in the host galaxy (see Phillips et al. (2013)). Thus, it is interesting to infer size distribution of interstellar grains that reproduce such low values of R_V .

Polarimetric studies of SNe Ia have opened a new window into probing dust properties and grain alignment in the galaxies because the intrinsic polarization of SNe light is negligible (see Wang & Wheeler 2008 for a review). Four SNe Ia with high quality of polarization data (SNe 1986G, 2006X, 2008fp, 2014J) exhibit anoma-

* E-mail: hoang@cita.utoronto.ca

lous polarization curves that rise toward UV wavelengths (Kawabata et al. 2014; Patat et al. 2015). Fitting the observational data with the typical ISM polarization law–Serkowski law–yields an anomalous value of peak wavelength ($\lambda_{\max} < 0.2 \mu\text{m}$) for SNe 2008fp and 2014J, which is much lower than the typical value $\lambda_{\max} \sim 0.55 \mu\text{m}$ in the Galaxy. For comparison, available data for Galactic polarization show the lowest peak wavelengths $\lambda_{\max} = 0.33 \mu\text{m}$ and $0.35 \mu\text{m}$ for Cyg OB2 No. 10 and 12 (Whittet et al. 1992), and $\lambda_{\max} < 0.35 \mu\text{m}$ for HD 193682 (Anderson et al. 1996).

The question of which origin (IS dust or CS dust) for these anomalous values of R_V and λ_{\max} remains unclear, and addressing this question has important implication for the progenitors of SNe Ia. If IS dust is important as suggested in previous studies (Phillips et al. 2013; Patat et al. 2015), the anomalous values could reflect peculiar properties of dust and alignment of grains in intervening clouds along the lines of sight to SNe or perhaps in the average IS dust of the hosted galaxies (Phillips et al. 2013; Patat et al. 2015). In this paper, we will use inversion technique (Section 4) to infer best-fit grain size distribution and alignment function, in order to understand dust properties and alignment underlying the anomalous features.

The structure of the paper is as follows. In Section 2 we present observational data for the selected SNe Ia compiled from the literature. Section 3 is devoted to present theoretical models of extinction and polarization and observational constraints. In Section 4 we briefly describe our inversion technique and obtained results. Extended discussion on dust properties and grain alignment mechanisms responsible for anomalous polarization are presented in Section 5. A short summary is given in 6.

2 OBSERVED EXTINCTION AND POLARIZATION DATA

2.1 Extinction and Polarization of Starlight in the Milky Way

Interstellar dust causes extinction of starlight, which can be described by Cardelli et al. (1989) (CCM) extinction law with $R_V \sim 3.1$. In addition, the alignment of non-spherical grains with interstellar magnetic fields produces differential extinction of starlight, resulting in starlight polarization, and thermal emission from aligned dust grains become linearly polarized (see Andersson et al. 2015; Lazarian, Andersson, & Hoang 2015 (LAH15) for latest reviews).

The wavelength-dependence polarization (hereafter polarization curve) induced by IS dust is approximately described by the Serkowski law (Serkowski et al. 1975):

$$P_{\text{is}}(\lambda) = P_{\max} \exp \left[-K \ln^2 \left(\frac{\lambda_{\max}}{\lambda} \right) \right], \quad (1)$$

where P_{\max} is the maximum polarization at wavelength λ_{\max} , and K is a parameter depending on λ_{\max} (Wilking et al. 1980). For the Galaxy, $\lambda_{\max} \sim 0.55 \mu\text{m}$, although some lines of sight (LOS) exhibit lower λ_{\max} . But to date, the low values of $\lambda_{\max} < 0.4 \mu\text{m}$ have not been detected (see Andersson & Potter 2007).

2.2 SNe 1986G and 2006X

SN 1986G exploded in a dust lane in the host galaxy NGC 5128 (Cen A), which was found to have at least a dozen of distinct clouds along the line of sight (D’Odorico et al. 1989; Cristiani et al. 1992). Optical and near-IR photometric observations show that the extinction of SN 1986G can be described by the CCM law with $R_V = 2.57$ (see Phillips et al. 2013). Polarimetric measurements were first reported in Hough et al. (1987), in which the polarization curve is well fitted by the Serkowski law with $\lambda_{\max} = 0.43 \mu\text{m}$. It was suggested that interstellar grains in the dust lane are aligned with the local magnetic field but with the alignment efficiency lower than that in the Milky Way.

SN 2006X exploded within or behind the disk of NGC 4321 normal galaxy in Virgo cluster. Photometric observations in optical and near-infrared by Wang et al. (2008) reveal an unusually low value of $R_V \approx 1.5$. Polarimetric data (Patat et al. 2009) show a low value of $\lambda_{\max} \sim 0.365 \mu\text{m}$. It was suggested that the bulk of the polarization is produced by aligned grains within a single dense molecular cloud in the host galaxy ISM (Cox & Patat 2008; Phillips et al. 2013; Patat et al. 2015). Therefore, for SNe 1986G and 2006X, in the following, we assume the entire extinction and polarization are produced by IS dust.

2.3 SNe 2008fp and 2014J

2.3.1 Anomalous values of R_V and λ_{\max}

SN 2008fp is located in the host galaxy ESO 428-G14, a peculiar galaxy with an active nucleus. Similar to SN 2006X, SN 2008fp exhibits an extreme value $R_V \sim 1.2$ (Phillips et al. 2013; Cox & Patat 2014). Its polarization data also demonstrate an anomalous value of $\lambda_{\max} \sim 0.15 \mu\text{m}$ (Cox & Patat 2014). It is believed that the extinction and polarization for SN 2008fp are mainly produced by IS dust due to the lack of variability in the absorption line profile and strong CN interstellar absorption features (Cox & Patat 2014).

SN 2014J is located in the host galaxy NGC 3034 (M82), which was discovered accidentally by a group of students (Fossey et al. 2014). Photometric observations using Swift near-UV and optical-near IR data by Brown et al. (2015) show that the reddening of SN 2014J can be best fitted by the CCM law with $R_V = 1.4$ (see also Welty et al. 2014; Amanullah et al. 2015). Polarimetric observations show a even more extreme value of $\lambda_{\max} = 0.05 \mu\text{m}$ (Patat et al. 2015; see also Kawabata et al. 2014).

Foley et al. (2014) show that the best-fit models for the extinction toward SN 2014J require both CS dust and IS dust, and each contributes equally to the observed reddening. Their best-fit parameters for the interstellar reddening is $R_V = 2.59$ and $E_{B-V} = 0.45 \text{ mag}$ (i.e., $A_V = 1.165 \text{ mag}$), and CS dust contributes about the half extinction. On the other hand, appealing to the well-aligned polarization angles with the local spiral arms of the host galaxies and small variability before and after the maximum epoch, Patat et al. (2015) argued that IS dust is a dominant contribution to the observed polarization, although adding the contribution of CS dust, they obtained a more reasonable R_V and λ_{\max} for this case.

2.3.2 Two-component extinction/polarization model

Due to uncertainty in the origin of anomalous R_V and λ_{\max} in SNe 2008fp and 2014J, we consider two models 1 and 2. Model 1 assumes that the entire extinction and polarization are produced by IS dust (one dust component), whereas model 2 considers two dust components (IS and CS dust) contributing to the observed data.

The observed extinction from both IS and CS dust is given by

$$A_{\text{obs}}(\lambda) = A_{\text{is}}(\lambda) + A_{\text{cs}}(\lambda), \quad (2)$$

where $A_{\text{is}}(\lambda)$ is given by the CCM law, and the latter is a power law (Goobar 2008):

$$(A(\lambda)/A_V)_{\text{cs}} = 1 - \alpha + \alpha \left(\frac{0.55 \mu\text{m}}{\lambda} \right)^q, \quad (3)$$

where α and q are free parameters.

Let f_{cs} is the fraction of the total observed visual extinction A_V contributed by CS dust. Then, we can obtain the followings

$$A_{\text{cs}}(\lambda) = f_{\text{cs}} A_V \times (A(\lambda)/A_V)_{\text{cs}}, \quad (4)$$

$$A_{\text{is}}(\lambda) = (1 - f_{\text{cs}}) A_V \times (A(\lambda)/A_V)_{\text{is}}. \quad (5)$$

Similarly, including the polarization due to Rayleigh scattering by CS dust (see Andersson et al. 2013 for details), the observed polarization is then equal to

$$P_{\text{obs}}(\lambda) = P_{\text{is}}(\lambda) + P_{\text{cs}} \left(\frac{\lambda}{0.4 \mu\text{m}} \right)^{-4}, \quad (6)$$

where $P_{\text{is}}(\lambda)$ is the polarization from IS dust (Eq. 1), and P_{cs} denotes the polarization due Rayleigh scattering.

To infer the best-fit model parameters α , q , f_{cs} , and R_V , we use the publicly available package lmfit-py¹ to fit $A_{\text{obs}}(\lambda)$ to the observed extinction. Similarly, we fit $P_{\text{obs}}(\lambda)$ to the observed polarization to find P_{cs} , λ_{\max} , P_{\max} , and K . Our fits using the two-component model return reasonable parameters with $R_V \approx 2.2$ for IS dust contributing $A_V = 0.29$ to the total extinction, $\lambda_{\max} = 0.41 \mu\text{m}$, and $K = 1.03$ (see details in Figure 1 for SN 2008fp). We also rerun for SN 2014J and obtain a good fit with the comparable parameters as in previous works (Foley et al. 2014; Patat et al. 2015).

3 DUST MODEL AND OBSERVATIONAL CONSTRAINTS

3.1 Dust Model

We adopt a mixed-dust model consisting of astronomical silicate grains and graphite grains (see Weingartner & Draine 2001; Draine & Li 2007). Because graphite grains are unlikely aligned with the magnetic field (Chiar et al. 2006; see LAH15 for a review), we assume that only silicate grains are aligned while carbonaceous grains are randomly oriented. Oblate spheroidal grains with axial ratio $r = 2$ are considered.

The extinction of starlight induced by randomly oriented grains in units of magnitude is given by

$$A(\lambda) = \sum_{j=\text{sil,carb}} 1.086 \int \int C_{\text{ext}}^j(a) \left(\frac{dn^j}{da} \right) dadz, \quad (7)$$

¹ <http://cars9.uchicago.edu/software/python/lmfit/index.html>

where a is the effective grain size defined as the radius of an equivalent sphere of the same grain volume, dn^j/da is the grain size distribution of dust component j , C_{ext} is the extinction cross-section, and the integration is taken along the entire line of sight z .

The degree of polarization (in unit of %) of starlight due to differential extinction of aligned grains along the line of sight is computed by

$$P(\lambda) = \sum_{j=\text{sil,carb}} 100 \int \int \frac{1}{2} C_{\text{pol}}^j(a) f^j(a) \frac{dn^j}{da} dadz, \quad (8)$$

where C_{pol} is the polarization cross-section, and $f^j(a)$ is the effective degree of grain alignment for dust component j with size a (hereafter alignment function). Here we take C_{ext} and C_{pol} computed for different grain sizes and wavelengths from Hoang et al. (2013).

3.2 Observational Constraints

3.2.1 Gas-to-dust ratio

The important constraint of the dust model is the gas-to-dust mass ratio, which ensures that the total gas mass relative to the total dust mass must be constrained by observations. The gas-to-dust mass ratio is usually represented through N_{H}/A_V where N_{H} is the gas column density. For the Galaxy, measurements give $N_{\text{H}}/E_{B-V} = 5.8 \times 10^{21} \text{ cm}^{-2} \text{ mag}^{-1}$, which corresponds to $N_{\text{H}}/A_V = 5.8 \times 10^{21} \text{ cm}^{-2} \text{ mag}^{-1}/R_V$.

The gas-to-dust mass ratio for the SN 1986G hosted galaxy is measured by Herschel (Parkin et al. 2012) and SINGS (Draine et al. 2007). The former provides an average gas-to-dust mass ratio to be 103 ± 8 , which is similar to our Galaxy. Therefore, we can take the same ratio of the Galaxy, $N_{\text{H}}/E_{B-V} = 5.8 \times 10^{21} \text{ cm}^{-2} \text{ mag}^{-1}$, for the LOS to SN 1986G with $E_{B-V} = 0.79 \text{ mag}$. It is worth mentioning that D'Odorico et al. (1989) estimated $N_{\text{H}} \sim 5 \times 10^{21} \text{ cm}^{-2}$ for $E_{B-V} = 0.9 \pm 0.1 \text{ mag}$.

The reddening to SN 2006X is estimated to be $E_{B-V} = 1.42 \pm 0.4 \text{ mag}$, assuming the Galactic foreground equal to 0.026 mag. Observations for NGC 4321 in Draine et al. (2007) show that the dust-to-gas ratio is about two times higher than that of our Galaxy with metallicity comparable to the Solar abundance. Therefore, for SN 2006X, we assume $N_{\text{H}}/A_V = 5.8 \times 10^{21} \text{ cm}^{-2} \text{ mag}^{-1}/2R_V$, or $N_{\text{H}}/E_{B-V} = 2.9 \times 10^{21} \text{ cm}^{-2} \text{ mag}^{-1}$ for $R_V = 1.31$.

For SN 2008fp, Cox & Patat 2014 estimated $N(\text{H}_1) = 6.2_{-2.1}^{+3.2} \times 10^{20} \text{ cm}^{-2}$, and $N(\text{H}_2) = 7.2_{-2.7}^{+4.8} \times 10^{20} \text{ cm}^{-2}$, which gives $N_{\text{H}} = N(\text{H}_1) + 2N(\text{H}_2) = 2.1 \times 10^{21} \text{ cm}^{-2}$. For model 1, we get $N_{\text{H}}/A_V = 2.95 \times 10^{21} \text{ cm}^{-2} \text{ mag}^{-1}$ for $A_V = 0.71 \text{ mag}$. For $R_V = 1.2$, it yields $N_{\text{H}}/E_{B-V} = 3.52 \times 10^{21} \text{ cm}^{-2} \text{ mag}^{-1}$, indicating that the dust-to-gas ratio in this galaxy is higher than that in the Galaxy. For model 2 in which the scattering by IS dust is included, the ratio becomes $N_{\text{H}}/E_{B-V} = 1.6 \times 10^{22} \text{ cm}^{-2} \text{ mag}^{-1}$ for $E_{B-V} = 0.13 \text{ mag}$.

For SN 2014J, the gas column density is estimated to be $\log N_{\text{H}} = 21.53 \pm 0.13$ (see Table 3 in Ritchey et al. (2014)). Thus, $N_{\text{H}}/E_{B-V} = 2.47 \times 10^{21} \text{ cm}^{-2} \text{ mag}^{-1}$ for model 1 with $E_{B-V} = 1.37 \text{ mag}$. For model 2 in which IS dust only contributes $E_{B-V} = 0.45$ (Foley et al. 2014), we obtain $N_{\text{H}}/E_{B-V} = 7.52 \times 10^{21} \text{ cm}^{-2} \text{ mag}^{-1}$.

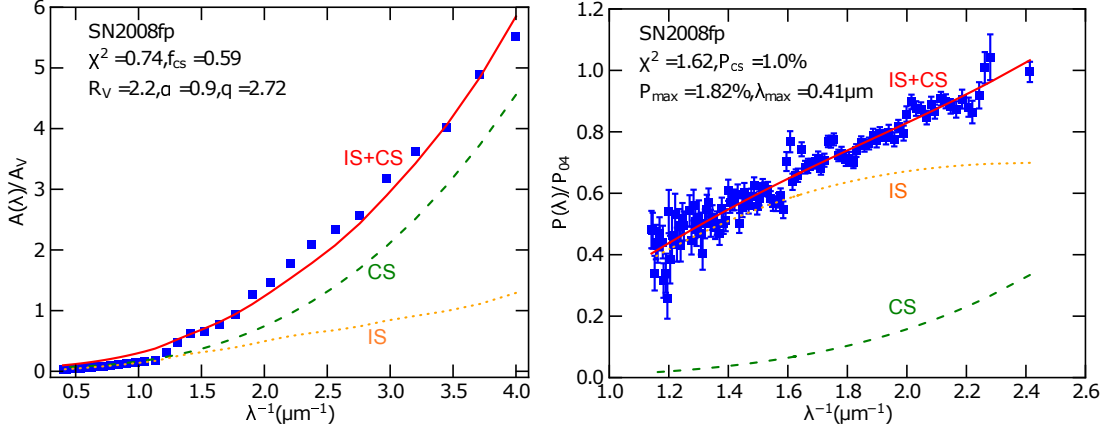


Figure 1. Two-component extinction (left) and polarization (right) fits to the observational data of SN 2008fp taken from (Patat et al. 2015). Dotted and dashed lines represent the results for IS dust and CS dust, respectively, and solid lines show the total contribution from the two components.

Table 1. Physical parameters for SNe Ia

SNe	Host	Host type	$\lambda_{\max}(\mu\text{m})$	$p_{04}(\%)$	K	R_V	$A_V(\text{mag})$	$E_{B-V}(\text{mag})$	N_H/E_{B-V} ($\text{cm}^{-2} \text{mag}^{-1}$)
1986G	NGC5128	starburst	0.43	5.1	1.15	2.57	2.03	0.79	5.8E+21
2006X	NGC4321	normal	0.36	7.8	1.47	1.31	1.88	1.44	2.9E+21
2008f(mod 1)	ESO428-G14	Seyfert	0.15	2.6	0.40	1.20	0.71	0.59	3.5E+21
2008f(mod 2)	–	–	0.41	1.8	1.03	2.20	0.29	0.13	1.6E+22
2014J(mod 1)	NGC3034	starburst	0.05	6.6	0.40	1.40	1.85	1.37	2.5E+21
2014J(mod 2)	–	–	0.35	3.7	1.15	2.59	1.17	0.45	7.5E+21

In Table 1 we summarize basic parameters of four SNe Ia used for inversion problem (see also Patat et al. 2015).

3.2.2 Metal abundances in galaxies

One important constraint is the fraction of metal elements (e.g., Si, Fe, Mg, and C) incorporated into dust. Let us now evaluate the silicate volume per H atom. Assuming that all Mg, Si and Fe budget (Anders & Grevesse 1989) are incorporated in the solid silicate material, then, for each Si atom, we would form a structure $Mg_{1.1}Fe_{0.9}SiO_4$. The volume of silicate material per H atom is $V_{\text{sil},0}/H = (Si/H)m_{\text{sil}}/\rho_{\text{sil}} = 2.57 \times 10^{-27} \text{ cm}^3/H$ for $\rho_{\text{sil}} = 3.5 \text{ g cm}^{-3}$. Similarly, for graphite with $\rho_{\text{gra}} = 2.2 \text{ g cm}^{-3}$, we get $V_{\text{gra},0} = 2.23 \times 10^{-27} \text{ cm}^3/H$ with $C/H = 2.46 \times 10^{-4}$. The volume of j dust component of the model is evaluated by $V_j = \int (4\pi a^3/3) dn_j/da$.

4 MONTE CARLO INVERSION TECHNIQUE AND RESULTS

Inversion technique has frequently been used to infer the grain size distribution (Kim et al. 1994; Larson et al. 2000; Zubko et al. 2004) of dust in the ISM of the Milky Way, and in nearby galaxies (e.g, small Magellanic cloud (Clayton et al. 2003). Draine & Fraisse (2009)

used Levenberg-Marquart method to infer both the grain size distribution and alignment function. Here we follow Hoang et al. (2013, 2014) (hereafter HLM13, HLM14) using the Monte Carlo method to find best-fit grain size distribution and alignment function for interstellar grains in the SNe Ia hosted galaxies with anomalous extinction and polarization data.

4.1 Monte Carlo Simulation-based Inversion Technique

To study dust properties and grain alignment toward SNe Ia, we will find the best-fit grain size distribution and alignment function by fitting the observed extinction and polarization curves with the theoretical models A_{mod} and p_{mod} (Equations (7) and (8)). The observed data for the SNe Ia are calculated using Equation (1) and the CCM law with the relevant parameters shown in Table 1. Our nonlinear least square fitting code uses Monte Carlo simulation method to minimize an objective function $\chi^2 = \chi_{\text{mod}}^2 + \chi_{\text{con}}^2$ where $\chi_{\text{mod}}^2 = \chi_{\text{ext}}^2 + \chi_{\text{pol}}^2$ describes the misfit between the model extinction and polarization and the observed data, and χ_{con}^2 describes the model constraints, including the smoothness of dn/da and the monotonic variation of f_a (see HLM13, HLM14 for details).

The important constraint for the polarization model

and the alignment function $f(a)$ is that, for the maximum polarization efficiency $p_{\max}/A(\lambda_{\max}) = 3\% \text{ mag}^{-1}$ (see [Draine 2003](#) for a review), we expect that the conditions for alignment are optimal, which corresponds to the case in which the alignment of big grains can be perfect, and the magnetic field is regular and perpendicular to the line of sight. Thus, we set $f(a = a_{\max}) = 1$. For a given line of sight with lower $p_{\max}/A(\lambda_{\max})$, the constraint $f(a = a_{\max})$ should be adjusted such that $f(a = a_{\max}) = (1/3)p_{\max}/A(\lambda_{\max})$. For big grains, we expect the monotonic increase of $f(a)$ versus a , thus a monotonic constraint is introduced for $a > 50\text{\AA}$. For $a < 50\text{\AA}$, expecting a different alignment mechanism based on resonance paramagnetic relaxation that results in a peaky alignment function (HLM13), we don't constrain the monotonic decrease for this very small grains. Other constraints include the non-smoothness of dn/da and $f(a)$ (see [Draine & Allaf-Akbari 2006](#)).

Because extinction and polarization data in far-UV wavelength ($\lambda < 0.25\text{ }\mu\text{m}$) toward these SNe Ia are unavailable, we will not attempt to invert the data for the far-UV range, which is mainly contributed by ultrasmall grains (including polycyclic aromatic hydrocarbons). Thus, we consider $\lambda = 0.25 - 2.5\text{ }\mu\text{m}$ and compute the extinction and polarization model (Equations (7) and (8), respectively). We use 64 bins of grain size in the range $a = 10\text{\AA}$ to $1\text{ }\mu\text{m}$ and 64 bins of the wavelength.

The fitting procedure is started with an initial size distribution $n(a)$ that best reproduces the observational data for the typical ISM (model 3 in [Draine & Fraisse 2009](#)) and is iterated until the convergence criterion is satisfied. At each iteration step, for each size bin, we generate 32 independent sample models by perturbing all model parameters n_a, f_a using Gibbs sampler, and retain the best model determined by the current minimum χ^2 . The process is looped over all size bins and the final minimum χ^2 is obtained for which a unique best-fit model is retained. An iteration step is accomplished. The convergence criterion is based on the decrease of χ^2 after one step: $\epsilon = (\chi^2(n, f) - \chi^2(\tilde{n}, \tilde{f}))/\chi^2(n, f)$. If $\epsilon \leq \epsilon_0$ with ϵ_0 sufficiently small, then the convergence is said to be achieved (see HLM13, HLM14). With the value $\epsilon_0 = 10^{-3}$ adopted, the convergence is slow for some lines of sight, we stop the iteration process when the variation of χ^2 is relatively stable.

4.2 Inversion Results

4.2.1 Convergence and Best-fit models

For SNe 1986G, 2006X, we run the inversion code assuming the entire reddening and polarization are produced by interstellar dust, and obtain a gradual reduction of χ^2 . For SNe 2008fp and 2014J, we run the inversion code for both model 1 and model 2 (see Table 1). For SN 2014J (model 1), our simulations do not show the reduction of χ^2 and the minimum chi-square obtained is too large (i.e., $\chi^2 \sim 10^2$), which indicates that the inversion fails to converge. For model 2, our simulations exhibit a good reduction of χ^2 . Detailed evolution of χ^2 and χ^2_{mod} vs. the iteration step for four SNe Ia are shown in Figure 2.

From the figure, it can be seen that the achieved goodness of fits is excellent for SN 1986G and SN 2014J (model 2), which have terminal $\chi^2_{\text{mod}} \sim 0.3 - 0.4$. For the case with

extreme R_V , SN 2006X, the goodness of fit is poorer with $\chi^2_{\text{mod}} \sim 3$. SN 2008fp (model 1) with both extreme R_V and λ_{\max} has rather slow reduction in χ^2 , which requires 100 iteration steps to reach the stable value of χ^2 . Interestingly, SN 2008fp (model 2) shows similar trend as model 1, but reaches higher terminal χ^2 .

Figure 3 shows best-fit models to the observed extinction (left panels) and polarization curves (right panels) for SNe 1986G and 2006X, SNe 2008fp, and 2014J.

4.2.2 Best-fit grain size distribution and alignment function

Figure 4 shows the best-fit model parameters for our considered SNe Ia, including grain mass distribution and alignment function. The best-fit mass distributions show the lack of large grains $a > 0.1\text{ }\mu\text{m}$. For instance, compared to SN 1986G, SN 2006X with a much lower value of R_V requires a significant increase in the abundance of small silicate grains at $a \sim 0.06\text{ }\mu\text{m}$. In particular, both SNe 1986G and 2006X have slightly different best-fit alignment functions. In addition, the alignment of small grains $a \sim 0.05 - 0.1\text{ }\mu\text{m}$ is significantly increased compared to the typical alignment function in the Galaxy with $\lambda_{\max} \sim 0.55\text{ }\mu\text{m}$ (e.g., see HLM14), which is required to reproduce the low values of $\lambda_{\max} \sim 0.35 - 0.45\text{ }\mu\text{m}$.

Figure 4 (lower panels) shows the results for SNe 2008fp (models 1 and 2) and 2014J (model 2). Compared to SN 2006X with similar, low value of R_V , SN 2008fp (model 1) requires the higher mass of very small silicate grains at $a < 0.010\text{ }\mu\text{m}$ but lower mass of small silicate grains $a \sim 0.06\text{ }\mu\text{m}$. Similarly, the mass of small graphite grains must be enhanced to compensate for the reduction of small silicate in order to reproduce the same R_V as SN 2006X. Interestingly, for SN 2008fp (model 1), the alignment degree is independent on the grain size, in which very small grains must be aligned as efficient as large grains. The best-fit size distribution and alignment function obtained for SN 2014J (model 2) are reminiscent of SN 1986G due to similar low R_V and λ_{\max} .

5 DISCUSSION

5.1 Dust properties toward SNe Ia: enhancement in the mass of small grains

To reproduce the anomalous extinction and polarization for four SNe Ia (1986G, 2006X, 2008fp, and 2014J), our best-fit models indicate that dust grains essentially have enhanced mass at small size $a < 0.1\text{ }\mu\text{m}$, whereas large grains $a > 0.1\text{ }\mu\text{m}$ are subdominant. This is essentially in agreement with previous works ([Wang et al. 2008](#); [Phillips et al. 2013](#); [Patat et al. 2015](#)). It is the first time a specific model of grain size distribution is presented to successfully reproduce the anomalous observational data.

In particular, SN 2006X with extreme value of $R_V = 1.31$ but low value of $\lambda_{\max} = 0.365\text{ }\mu\text{m}$ requires a largest enhancement in the mass of small grains of size $a \sim \lambda_{\max}/2\pi \sim 0.06\text{ }\mu\text{m}$ among the considered SNe Ia. This is easily understood because to reproduce extreme value R_V , it requires increased mass of small grains, but such additional mass must

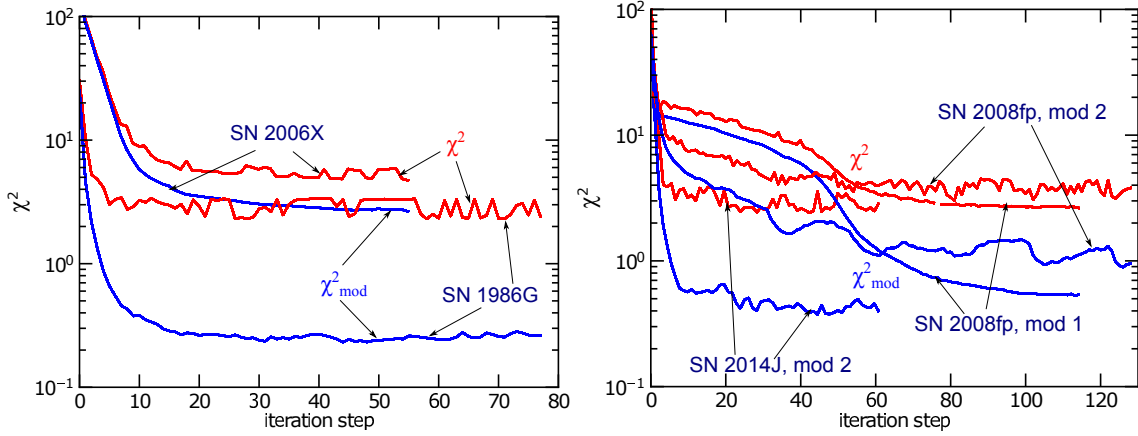


Figure 2. Reduction of total χ^2 and χ^2_{mod} (i.e., mistfit between the model and data only) vs. the iteration step for the SNe Ia considered. A fast steady reduction in χ^2 is achieved after about 30 steps for all cases except SN 2008fp.

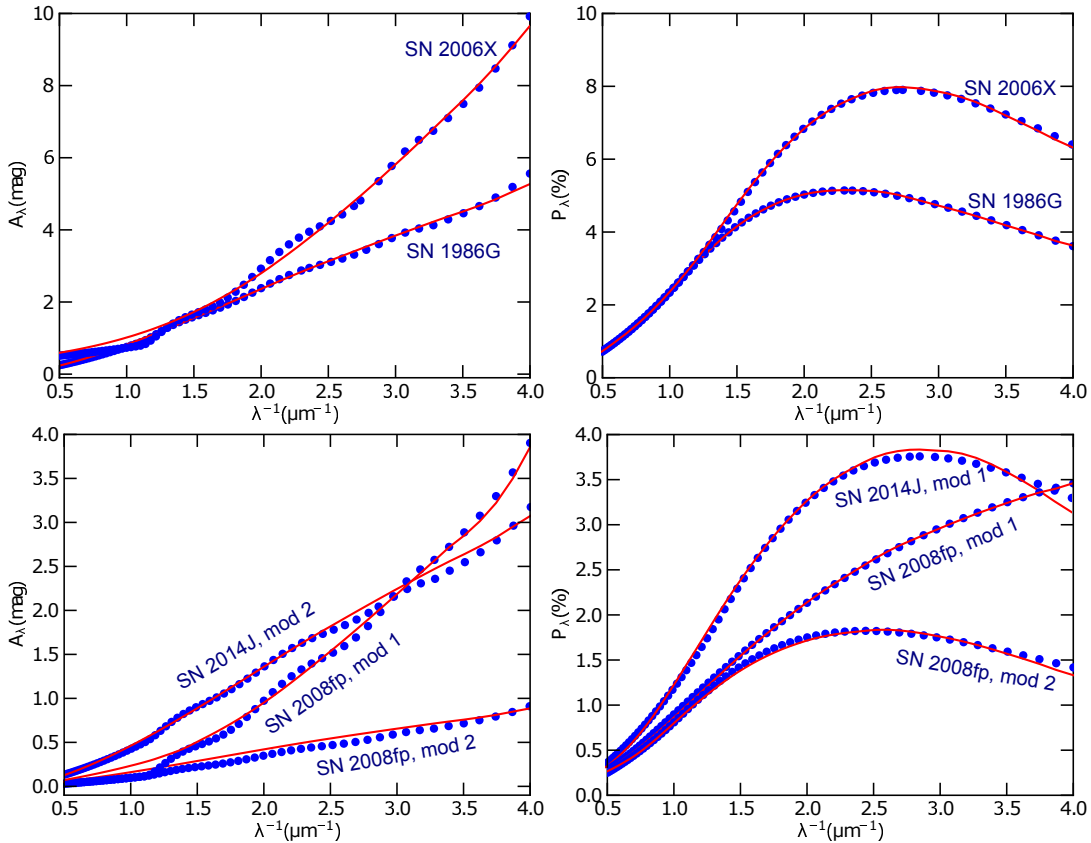


Figure 3. Best-fit models (solid lines) vs. observed data (circles) for extinction (left) and polarization (right) of SNe 1986G and 2006X. Excellent fit is obtained both for the polarization and extinction curves.

be well concentrated at not very small size to reproduce a low value of λ_{max} . The graphite mass fraction in this model is estimated to be $q_{\text{gra}} \sim 8\%$, about 3 times lower than that in the Galaxy ($q_{\text{gra}} \sim 20\%$), which indicates the decrease of the depletion of C into the grain. This result appears to be in agreement with the high abundance of gas phase C (about 2 times higher than for the Galaxy) reported by [Cox & Patat \(2014\)](#) based on the analysis of CN absorption lines from the dense cloud.

For SN 2008fp that exhibits both unusually low values

of R_V and $\lambda_{\text{max}} = 0.148 \mu\text{m}$ (model 1 without CS dust), our inversion results reveal a high mass fraction of carbonaceous grains (e.g. at $a \sim 0.04 \mu\text{m}$) and an efficient alignment of grains of all sizes. When including Rayleigh scattering by CS dust (model 2), we derived more reasonable parameters for the extinction and polarization curves (i.e., $R_V = 2.2$ and $\lambda_{\text{max}} = 0.42 \mu\text{m}$). As a result, our best-fit results do not reveal special grain alignment function as in model 1. This model also requires lower graphite mass

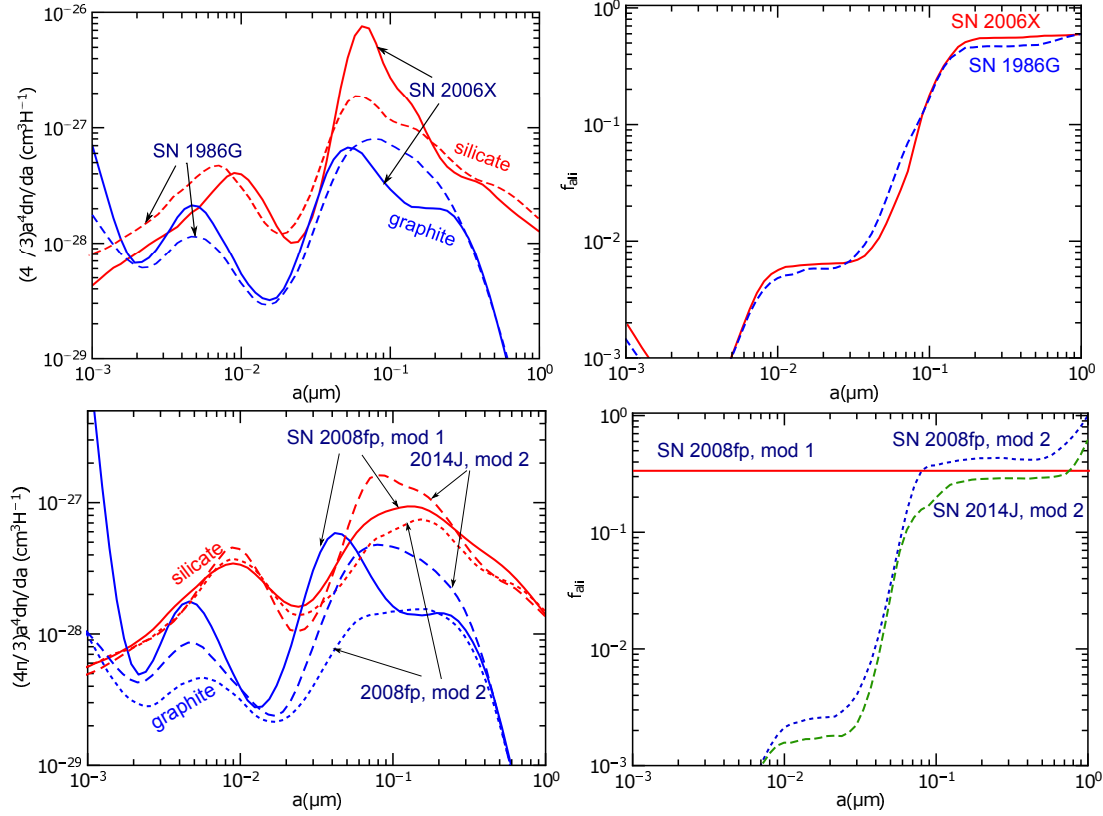


Figure 4. Grain mass distribution (red for silicate and blue for graphite) and alignment function for the best-fit models for the considered SNe Ia. SN 2006X exhibits a substantial enhancement in mass of small grains $a \sim 0.06 \mu\text{m}$ compared to SN 1986G. Three SNe 1986G, 2006X, 2008fp (model 2) and 2014J (model 2) have similar alignment functions with low alignment degree of small grains $a < 0.04 \mu\text{m}$. The alignment function of SN 2008fp (model 1) is peculiar.

fraction, $q_{\text{gra}} \sim 11\%$, which is consistent with estimates in Cox & Patat (2014).

For SN 2014J, our inversion for model 1 is unsuccessful, i.e., we cannot reach a target χ^2 (e.g., $\chi^2 < 10$). The inversion for model 2 is successful and provided a good fit to the observational data. The best-fit grain size distribution is similar to that in SN 1986G, which is expected due to its similar values of R_V and λ_{max} . So the best-fit alignment becomes closely similar to that of SNe 1986, 2006X and 2008fp (model 2), which indicate *universal* alignment function among the lines of sight to these SNe Ia.

Lastly, the remaining question is that why do the environments toward these SNe Ia have enhanced relative abundance of small grains?

High relative abundance of small grains may arise from several processes, including galaxy evolution, dust formation in SN II, asymptotic giant branch (AGB) stars, and dust evolution (see Patat et al. 2015). Small grains may be replenished by cloud-cloud collisions induced by SN radiation pressure.

Indeed, due to strong radiation pressure, grains in the cloud initially located closer to the explosion site are accelerated to high terminal velocities, as given by $v \simeq 171(L_{\text{bol}}/10^8 L_{\odot})^{1/2}(r_i/100 \text{ pc})^{-1/2}a_{-5}^{-1/2} \text{ km s}^{-1}$ (see Hoang et al. 2015). The ejecting cloud would collide with another cloud in its vicinity (e.g., for SN 1986G and 2014J), which results in destruction of big grains. It is noted that the drifting motion of fast grains through the gas undergo non-

thermal sputtering due to gas-grain collisions, which reduces the abundance of small grains. But this process usually takes a long time to be important, i.e., $\tau_{\text{sp}} \sim a\rho/n_{\text{gas}}v_{\text{gr}}m_{\text{H}} \sim 500a_{-5}\rho/3 \text{ g cm}^{-3}/(n_{\text{gas}}/100 \text{ cm}^{-3})(v_{\text{gr}}/100 \text{ km s}^{-1}) \text{ yr}$. These scenarios will result in the time variability of the extinction and polarization.

5.2 Grain alignment of interstellar dust toward the SNe Ia

5.2.1 Low values of $\lambda_{\text{max}} \sim 0.3 - 0.45 \mu\text{m}$

The polarization curves for SNe 1986G and 2006X exhibit low values of $\lambda_{\text{max}} \sim 0.3 - 0.45 \mu\text{m}$. For SNe 2008fp and 2014J, when accounting for the effect of Rayleigh scattering (model 2), we found that their values of λ_{max} become less extreme, as small as in SNe 1986G and 2006X. To reproduce such low values of λ_{max} , we find that the enhancement in relative abundance of small silicate grains is sufficient, while the alignment function does not exhibit special features in which the grains larger than $\sim 0.05 \mu\text{m}$ must be efficiently aligned (see Figure 4).

The question now is what alignment mechanisms are at work?

It is noted that both SNe 1986G and 2014J exploded in the disk of starburst galaxies NGC 5128 and NGC 3034, and there exist numerous clouds along the LOS. Therefore, the grain alignment in these cases would reflect the average

alignment properties of dust grains in the ISM. Due to strong star formation activity, the average starlight radiation in starburst galaxies is much stronger than the average ISRF in our solar neighborhood. As a result, interstellar grains toward SNe 1986G and 2014J can be aligned by radiative torques induced by starlight, which is similar to the Galaxy.

5.2.2 Extreme values of $\lambda_{\max} < 0.2 \mu\text{m}$: radiative torque alignment by radiation from SNe Ia

Among the SNe Ia considered, SN 2008fp is an exceptional case in which both model 1 and model 2 could reproduce the observational data. Indeed, model 1 without CS dust slightly provides a better fit (smaller χ^2), but its extreme value of $\lambda_{\max} = 0.15 \mu\text{m}$ requires very small grains $a_{\text{ali}} \sim 0.01$ also being aligned as efficient as big grains. This is unusual because small grains in the Galaxy are found to be weakly aligned (Kim & Martin 1995; HLM14), and it is important to understand whether such a special grain alignment is physically possible.

Over the past few years, we have witnessed significant progress in theoretical and observational studies of grain alignment, and radiative torques (RAT) alignment has become a leading mechanism for the alignment of interstellar grains (see Andersson et al. 2015 and Lazarian et al. 2015 for reviews). According to the RAT model, the alignment of irregular grains depends on a number of physical parameters, including the angle between the anisotropic direction of the radiation field and the magnetic field, the radiation energy density, mean wavelength of the radiation spectrum, grain size, and the local gas density and temperature (Lazarian & Hoang 2007; Hoang & Lazarian 2008, 2009). For a SN Ia of luminosity L_{SN} , the radiation energy density at distance d_{pc} in units of pc is given by

$$u_{\text{rad}} = \int u_{\lambda} d\lambda = \int \frac{L_{\lambda} e^{-\tau_{\lambda}}}{4\pi c d^2} d\lambda = 1.06 \times 10^{-7} \frac{L_8 e^{-\tau}}{d_{\text{pc}}^2} \text{ ergs cm}^{-3}, \quad (9)$$

where τ_{λ} is the optical depth induced by intervening dust, $L_8 = L_{\text{SN}}/10^8 L_{\odot}$, and τ is defined as $e^{-\tau} = \int L_{\lambda} e^{-\tau_{\lambda}} d\lambda / L_{\text{SN}}$.

Thus, the critical size of aligned grains by RATs, a_{ali} , is determined by the maximum angular momentum induced by RATs, which is equal to (see Lazarian & Hoang 2007; Hoang & Lazarian 2014):

$$\frac{J_{\text{max}}}{J_{\text{th}}} \approx 30 \hat{\gamma}_{\text{rad}} \hat{\rho}^{1/2} a_{-5}^{1/2} \left(\frac{10^3 \text{ cm}^{-3}}{n_{\text{H}}} \right) \left(\frac{20 \text{ K}}{T_{\text{gas}}} \right) \times \left(\frac{\bar{\lambda}}{1.2 \mu\text{m}} \right) \left(\frac{10^6 L_8 e^{-\tau}}{d_{\text{pc}}^2} \right) \left(\frac{\bar{Q}_{\Gamma}}{10^{-2}} \right) \left(\frac{1}{1 + F_{\text{IR}}} \right), \quad (10)$$

where J_{th} is the thermal angular momentum of grains at gas temperature, F_{IR} is the damping coefficient due to infrared emission, $\hat{\gamma}_{\text{rad}} = \gamma_{\text{rad}}/0.1$ with γ_{rad} the anisotropy degree of the radiation field (unity in our case), $\bar{\lambda}$ and \bar{Q}_{Γ} are the wavelength and RAT efficiency averaged over the entire radiation field spectrum, respectively. Here we disregard the effect of the ISRF, which is small compared to the SN radiation in the clouds close to the SN.

For interstellar grains with $a \ll \bar{\lambda}$, \bar{Q}_{Γ} is approximately

equal to (Hoang & Lazarian 2014)

$$\bar{Q}_{\Gamma} \simeq 2 \left(\frac{\bar{\lambda}}{a} \right)^{-2.7} \simeq 2.4 \times 10^{-3} \left(\frac{\bar{\lambda}}{1.2 \mu\text{m}} \right)^{-2.7} a_{-5}^{2.7}. \quad (11)$$

Grains are expected to be efficiently aligned when spun up to suprathermal speeds, which is determined by the criteria $J_{\text{max}} \geq 3J_{\text{th}}$ (see Hoang & Lazarian 2008). The timescale that RATs can spin-up grains to suprathermal rotation is equal to

$$\tau_{\text{spin-up}} \equiv \frac{J_{\text{th}}}{dJ/dt} = \frac{\tau_{\text{drag}}}{J_{\text{max}}/J_{\text{th}}} \simeq \frac{6.58 \times 10^4 a_{-5} n_1^{-1} T_2^{1/2} \text{ yr}}{J_{\text{max}}/J_{\text{th}}}, \quad (12)$$

where $\tau_{\text{drag}} \simeq 6.58 \times 10^4 a_{-5} n_1^{-1} T_2^{1/2} / (1 + F_{\text{IR}}) \text{ yr}$ with $n_1 = n_{\text{H}}/10 \text{ cm}^{-3}$ is the rotational damping time due to gas drag. Plugging numerical values, we get

$$\tau_{\text{spin-up}} \simeq 0.5 \left(\frac{d_{\text{pc}}^2}{L_8 e^{-\tau}} \right) \bar{\lambda}^{1.7} a_{-5}^{-2.2} \text{ day} \quad (13)$$

Radiation energy of SNe Ia is produced mostly by conversion of the kinetic energy of ejecta interacting with surrounding environments (i.e., shocked regions). Most of such energy is concentrated in UV-optical wavelengths, especially in early epochs after the explosion (see Brown et al. 2009). For simplicity, let assume that the emitting region can be approximately described by a black body of effective temperature T_{SN} . Thus, we can estimate $\bar{\lambda} = \int \lambda u_{\lambda}(T_{\text{SN}}) d\lambda / \int u_{\lambda}(T_{\text{SN}}) d\lambda$. This gives $\bar{\lambda} = 0.35 \mu\text{m}$ for $T_{\text{SN}} = 1.5 \times 10^4 \text{ K}$.

In Figure 5 we shows a_{ali} (upper panel) and $\tau_{\text{spin-up}}$ (lower panel) as functions of d_{pc} for different values of n_{H} and $L_8 e^{-\tau}$.

Figure 5 (upper) shows that small grains $a_{\text{ali}} \sim 0.01 \mu\text{m}$ in the cloud at distances $d \sim 20 \text{ pc}$ with the gas density $n_{\text{H}} \sim 250 \text{ cm}^{-3}$ (as estimated for SN 2008fp in Cox & Patat 2014) could be aligned. For a very dense cloud $n_{\text{H}} \sim 10^4 \text{ cm}^{-3}$, the cloud must be very close at $d \sim 3 \text{ pc}$ to have $a_{\text{ali}} \sim 0.02 \mu\text{m}$ for $L_8 e^{-\tau} < 1$. These small distances compared to the galaxy scale indicate that the clouds are close to the explosion site to reproduce the observed polarization.

One important feature of the RAT alignment is the spin-up time, which may be longer than the observation time since the explosion time. From Figure 5 it shows that for a cloud at distance $d \sim 1 - 10 \text{ pc}$ (i.e., well beyond the sublimation radius, see Hoang et al. 2015), the $\sim 0.03 \mu\text{m}$ grains can be radiatively aligned on $t_{\text{spin-up}} \sim 0.3 - 30$ days for $L_{\text{SN}} = 10^8 L_{\odot}$.

It is noted that polarimetric observations of SN 2008fp were performed on -2, 3, 9 and 31 days relative to the maximum epoch (Cox & Patat 2014). For SN 2014J, the observations were carried out on three epochs (Jan 28, Feb 3, Mar 8, 2014) with the maximum brightness in the first week of February (Patat et al. 2015). As a result, RAT alignment by the radiation from SNe requires the cloud be within 10 pc such that $t_{\text{obs}} > \tau_{\text{spin-up}}$.

Finally, if the RAT alignment by SNe Ia's radiation is at work, why do other SNe Ia not exhibit extreme values of λ_{\max} ? The first reason may be that this cloud is located further away than the single cloud in SN 2008fp, or the radiation from the central source is significantly reduced by larger optical depth τ arising from circumstellar dust (e.g. for SN 2014J) or intervening clouds.

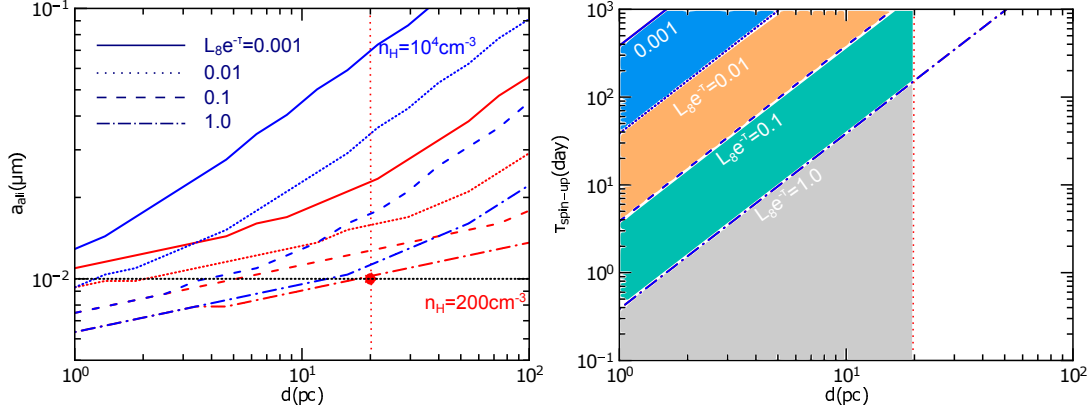


Figure 5. Upper panel: critical size of aligned grains a_{ali} by RATs as a function of the cloud distance d for different values of $L_8 e^{-\tau} = 10^{-3} - 1$. Two values of gas density $n_H = 200 \text{ cm}^{-3}$ (red) and 10^4 cm^{-3} (blue) are considered. Dotted vertical lines indicates the alignment $a_{\text{ali}} = 0.01 \text{ μm}$ for $L_8 e^{-\tau} = 1$ and $n_H = 200 \text{ cm}^{-3}$. Lower panel: spin-up time $\tau_{\text{spin-up}}$ for $a = 0.01 \text{ μm}$. Shaded areas mark the region where the RAT alignment of $a \geq 0.01 \text{ μm}$ grains can be observed for a given pair $L_8 e^{-\tau}$ and d_{pc} .

The RAT alignment of grains in the cloud is naturally applied to CS dust; the only difference is that in the latter the radiation from white dwarf (WD) induces grain alignment. Of course, the alignment of CS dust would result in the variability of polarization degree and dispersion angles through the SN explosion epochs.

5.2.3 Observational signatures of RAT alignment by SNe Ia's radiation

The variability of the SN luminosity results in the variation of a_{ali} , which certainly induces the variation of the polarization curves. To illustrate such an effect, we compute a number of polarization curves by varying a_{ali} , where a typical grain size distribution of the Galaxy (Draine & Li 2007) is chosen. The alignment function is assumed to be $f_a = 1 - \exp[-(a/a_{\text{ali}})^3]$, which captures our best-fit alignment functions shown in Figure 4. Obtained results are shown in Figure 6. It is shown that, when a_{ali} is decreased from 0.03 μm to 0.001 μm , the polarization at $\lambda < 0.4 \text{ μm}$ varies substantially, whereas its variation at $\lambda > 0.4 \text{ μm}$ is rather small.

The increase and decrease of the polarization at $\lambda < 0.4 \text{ μm}$ before and after the maximum luminosity epoch is a unique signature of RAT alignment toward SNe. Therefore, observing the far-UV SN polarization would provide important insight into the origin of anomalous polarization and the RAT alignment mechanism. Because the IS polarization is determined by the interstellar magnetic fields, the polarization angles are stable through the different epochs of SN observations. Thus, this model of RAT alignment naturally explains the lack of the variability of polarization vectors (see Patat et al. 2015).

5.3 Circumstellar dust and implications for SNe Ia progenitors

Using inversion technique, we found that the presence of CS dust in SN 2008fp is uncertain because our inversion is successful for both models without and with CS dust. Including CS dust allows us to get dust parameters R_V , λ_{max}

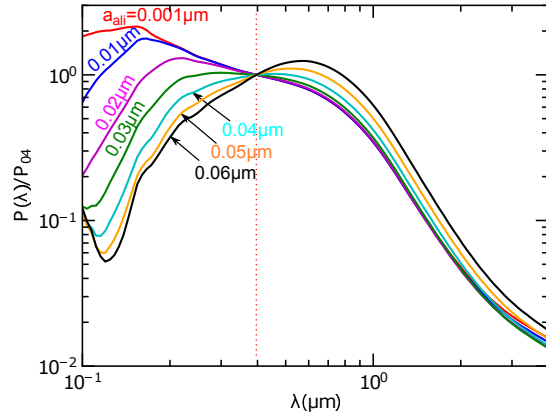


Figure 6. Normalized polarization curves predicted for different values of a_{ali} : peak wavelength shifts to blue when a_{ali} is decreased. Contribution of very small grains $a \leq 0.03 \text{ μm}$ are negligible for the polarization at $\lambda \geq 0.4 \text{ μm}$.

to be similar for four SNe Ia, and the alignment function of the IS dust toward these SNe Ia appears to be similar. However, it is argued that CS dust is unlikely important for SN 2008fp due to the lack of variability in the polarization angles (Patat et al. 2015) as well as the lack of variability of extragalactic absorption line profiles (see Cox & Patat 2014).

On the other hand, the existence of CS dust in SN2014J is favored by the fact that only the model with CS dust is successful, in which the CS dust contributes about one-half of the total extinction/polarization. This is in agreement with a recent analysis of M82 region before SN 2014J by Hutton et al. (2015) that supports the contribution of both CS dust and IS dust for low R_V .

Patat et al. (2015) argued that the presence of CS dust in SN 2014J is not ruled out (see also Foley et al. 2014), although the lack of variability in the polarization degree and polarization angles is difficult to reconcile. The authors suggested that the lack of such variability can be reproduced if the orientation of CS dust incidentally is not different from the magnetic field of the host galaxy, such that the polarization angles from scattering and IS dust become similar.

The indicated need for a Rayleigh scattering term in the modeling of SNe 2014J and probably 2008fp raises several observational issues, primarily one of source geometry. In all of the observed sources, the position angle (PA) of the polarization is found to be constant over the observed wavelength range. In other sources with combined dichroic and scattering polarization (e.g. IC 63 #75 and 17 Tau; [Andersson et al. 2013](#); [Matsumura et al. 2011](#)) the PA changes with wavelength. This constancy of PA for SN Ia polarization indicates that the origins of the dichroic (orientation of magnetic fields) and scattering (small dust grains relative to the illuminating source) polarization must be physically related. Over galactic scales such co-alignments are difficult to envision. B-G Andersson (private communications) suggested a phenomenological toy model, which illustrates the kind of source structure that would be needed to explain the observations. In this mode, the WD magnetosphere contains dust grains of typical Galactic size distribution, and an accretion disk in the magnetic equatorial plane contains small grains. The former grains can be aligned with the dipole magnetic field by radiation from the WD photosphere, whereas small dust grains undergo Rayleigh scattering, for which both processes result in parallel polarization vectors. This special geometry configuration can explain the invariability of the polarization angles. However, dust grains in accretion disk and magnetosphere will be swept away by SN ejecta shortly after the explosion.

Indeed, the WD magnetosphere is characterized by Alfvén radius at which the magnetic energy is balanced with the gas thermal energy, which is given by:

$$\begin{aligned} R_A &\sim (3B_\star^2 R_\star^6 / 2\dot{M} \sqrt{GM_\star})^{2/7}, \\ &\simeq 1.2R_\odot B_\star (kG)^{4/7} (\dot{M} / 10^8 \text{ g s}^{-1})^{-2/7} \\ &\quad \times (R_\star / 0.01R_\odot)^{12/7} (M_\star / 0.6M_\odot)^{-1/7}, \end{aligned} \quad (14)$$

where \dot{M} is the accretion rate, and B_\star is the magnetic field (see [Metzger et al. 2012](#)). For typical parameters $\dot{M} \sim 10^6 - 10^{10} \text{ g s}^{-1}$ and $B_\star \sim 1 - 100 \text{ kG}$, it yields $R_A \sim 0.3 - 62R_\odot \times (R_\star / 0.01R_\odot)^{12/7} (M_\star / 0.6M_\odot)^{-1/7}$.

It can be seen that dust grains within the magnetosphere would be swept away after $t \simeq 100R_\odot / v_{ej} \sim 2.1(v_{ej} / 0.03c)^{-1} \text{ hr}$, where the ejecta velocity during the free-expansion period is $v_{ej} \sim 10^4 \text{ km s}^{-1}$. As a result, observations at hours after the SN explosion would not see any signatures of such dust.

5.4 Magnetic alignment and Implication for magnetic fields in host galaxies

It is worth to mention an alternative paramagnetic alignment mechanism that is proposed by [Davis & Greenstein \(1951\)](#) to explain starlight polarization. However, paramagnetic alignment of thermally rotating small grains is found to be inefficient ([Lazarian 1997](#); [Hoang et al. 2014](#)). Without suprathermal rotation, even grains with superparamagnetic inclusions are far from being efficiently aligned ([Roberge & Lazarian 1999](#); [Hoang & Lazarian 2015](#), submitted). The joint action of RATs and superparamagnetic inclusions would result in the perfect alignment of sufficiently large grains ([Lazarian & Hoang 2008](#)).

[Hoang et al. \(2014\)](#) found that increasing the strength of magnetic fields can produce enhancement of alignment

of small grains, which partly results in the low values of λ_{max} and account for the polarization excess in far-UV ($\lambda < 0.2 \mu\text{m}$). Considering the environment conditions of four SNe Ia under interest, we see that SNe 1986G and 2014J belong to the starburst galaxies, which usually exhibit stronger magnetic fields than normal galaxies ([Thompson et al. 2006](#)). Thus, the low λ_{max} may partly arise from the high magnetic fields as predicted by HLM14. If this is the case, far-UV polarization observations would provide useful constraints on the magnetic fields.

The interstellar magnetic field along the lines of sight toward SNe Ia likely undergoes wandering due to interstellar turbulence. In our inversion technique, the effect of magnetic field wandering is incorporated into the alignment function $f = \Phi R \cos^2 \beta$, where β is the angle between the mean field and the plane of the sky, and Φ describes the average fluctuations of the local field with the LOS. The maximum value of f is constrained such that $P_{\text{max}}/A(\lambda_{\text{max}}) = 3\%/mag$ corresponds to $f_{\text{max}} = 1$.

6 SUMMARY

In the present paper, we have studied the properties and grain alignment of interstellar dust in external galaxies through four SNe Ia. The main findings are summarized as follows:

1. Using inversion technique, we have obtained the best-fit grain size distributions and alignment functions that reproduce observational extinction and polarization data of four SNe Ia (1986G, 2006X, 2008fp, and 2014J) with anomalous values of R_V and λ_{max} .
2. The best-fit grain size distributions reveal that the mass enhancement of small ($a \sim 0.05 - 0.1 \mu\text{m}$) silicate grains with peak around $a \sim 0.06 \mu\text{m}$. Thus, the peak λ_{max} provides an important insight into where the most mass of aligned grains is concentrated, in addition to indicating the average size of aligned grains. It is suggested that the enhanced abundance of small grains may be due to cloud-cloud collisions induced by SN radiation pressure.
3. For model 1 of SN 2008fp (without CS dust) with low value of R_V and extreme value of $\lambda_{\text{max}} \sim 0.15 \mu\text{m}$, to reproduce the observational data, increasing the relative abundance of small grains is insufficient. We find that the alignment of very small grains ($a \sim 0.01 \mu\text{m}$) must be as efficient as big grains. Including the effect of CS dust, the alignment function becomes more reasonable, similar to that for SNe 1986G and 2006X. The fit is however not improved, and the existence of CS dust is still uncertain.
4. We have suggested a model of grain alignment based on radiative torques induced by direct, strong radiation from SNe, which can adequately explain the efficient alignment of very small grains for model 1 of SN 2008fp. Far-UV polarimetric observations would be useful to differentiate the effect of IS dust and CS dust based on its polarization spectra.
5. Unsuccessfully fitting the extinction and polarization data for SN 2014J when only IS dust is considered highlights the importance of CS dust. Taking this component into account, we have obtained a good fit for SN 2014J. This is an additional evidence for the existence of CS dust around SN 2014J.

ACKNOWLEDGMENTS

I am very grateful to B-G Andersson for useful discussions in the early stage of this work and insightful comments on the manuscript. I thank B-G Andersson for making the suggestion that the steep rise in the observed SNe Ia polarization spectra might be due to Rayleigh scattering in the circumstellar environment. T.H. thanks Peter G Martin for interesting discussions and Nguyen-Luong Quang for useful comments. T.H. was supported by Humboldt Fellowship at Ruhr Universität Bochum and Goethe Universität Frankfurt am Main.

REFERENCES

- Amanullah R., Johansson J., Goobar A., et al. 2015, MNRAS, 453, 3300
- Anders E., Grevesse N., 1989, *Geochimica et Cosmochimica Acta*, 53, 197
- Anderson C. M. et al., 1996, AJ, 112, 2726
- Andersson B.-G., Lazarian A., Vaillancourt J. E., 2015, *Annual Review of Astronomy and Astrophysics*, 53, 501
- Andersson B.-G. et al., 2013, ApJ, 775, 84
- Andersson B.-G., Potter S. B., 2007, ApJ, 665, 369
- Brown P. J. et al., 2009, AJ, 137, 4517
- Brown P. J. et al., 2015, ApJ, 805, 74
- Brown P. J. et al., 2014, arXiv.org, p. 2381
- Cardelli J. A., Clayton G. C., Mathis J. S., 1989, ApJ, 345, 245
- Chiar J. E. et al., 2006, ApJ, 651, 268
- Clayton G. C., Wolff M. J., Sofia U. J., Gordon K. D., Misselt K. A., 2003, ApJ, 588, 871
- Cox N. L. J., Patat F., 2008, A&A, 485, L9
- Cox N. L. J., Patat F., 2014, A&A, 565, A61
- Cristiani S. et al., 1992, A&A, 259, 63
- Davis L. J., Greenstein J. L., 1951, ApJ, 114, 206
- D’Odorico S., di Serego Alighieri S., Pettini M., Magain P., Nissen P. E., Panagia N., 1989, A&A, 215, 21
- Draine B. T., 2003, ARA&A, 41, 241
- Draine B. T., Allaf-Akbari K., 2006, ApJ, 652, 1318
- Draine B. T. et al., 2007, ApJ, 663, 866
- Draine B. T., Fraisse A. A., 2009, ApJ, 696, 1
- Draine B. T., Li A., 2007, ApJ, 657, 810
- Foley R. J. et al., 2014, MNRAS, 443, 2887
- Fossey S. J., Cooke B., Pollack G., Wilde M., Wright T., 2014, CBET, 3792, 1
- Goobar A., 2008, ApJ, 686, L103
- Hoang T., Lazarian A., 2008, MNRAS, 388, 117
- Hoang T., Lazarian A., 2009, ApJ, 697, 1316
- Hoang T., Lazarian A., 2014, MNRAS, 438, 680
- Hoang T., Lazarian A., Martin P. G., 2013, ApJ, 779, 152
- Hoang T., Lazarian A., Martin P. G., 2014, ApJ, 790, 6
- Hoang T., Lazarian A., Schlickeiser R., 2015, ApJ, 806, 1
- Hough J. H., Bailey J. A., Rouse M. F., Whittet D. C. B., 1987, MNRAS, 227, 1P
- Hutton S., Ferreras I., Yershov V., 2015, arXiv:1506.03821, p. 3821
- Kawabata K. S. et al., 2014, ApJ, 795, L4
- Kim S.-H., Martin P. G., 1995, ApJ, 444, 293
- Kim S.-H., Martin P. G., Hendry P. D., 1994, ApJ, 422, 164
- Larson K. A. et al., 2000, ApJ, 532, 1021
- Lazarian A., 1997, MNRAS, 288, 609
- Lazarian A., Andersson B.-G., Hoang T., 2015, in Kolokolova L., Hough J., Levasseur-Regourd A.-C., eds, *Polarimetry of stars and planetary systems*. (New York:Cambridge University Press)
- Lazarian A., Hoang T., 2007, MNRAS, 378, 910
- Lazarian A., Hoang T., 2008, ApJ, 676, L25
- Matsumura M., Kameura Y., Kawabata K. S., Akitaya H., Isogai M., Seki M., 2011, PASJ, 63, L43
- Metzger B. D., Rafikov R. R., Bochkarev K. V., 2012, MNRAS, 423, 505
- Nobili S., Goobar A., 2008, A&A, 487, 19
- Parkin T. J. et al., 2012, MNRAS, 422, 2291
- Patat F., Baade D., Höflich P., Maund J. R., Wang L., Wheeler J. C., 2009, A&A, 508, 229
- Patat F. et al., 2015, A&A, 577, A53
- Phillips M. M. et al., 2013, ApJ, 779, 38
- Riess A. G., Filippenko A. V., Challis P., et al. 1998, AJ, 116, 1009
- Ritchey A. M., Welty D. E., Dahlstrom J. A., York D. G., 2014, arXiv.org
- Roberge W. G., Lazarian A., 1999, MNRAS, 305, 615
- Serkowski K., Mathewson D. S., Ford V. L., 1975, ApJ, 196, 261
- Thompson T. A., Quataert E., Waxman E., Murray N., Martin C. L., 2006, ApJ, 645, 186
- Wang L., Wheeler J. C., 2008, *Annual Review of Astronomy and Astrophysics*, 46, 433
- Wang X., Li W., Filippenko A. V., Foley R. J., Smith N., Wang L., 2008, ApJ, 677, 1060
- Wang X. et al., 2008, ApJ, 675, 626
- Wang X., Wang L., Filippenko A. V., et al. 2012, ApJ, 749, 126
- Weingartner J. C., Draine B. T., 2001, ApJ, 548, 296
- Welty D. E., Ritchey A. M., Dahlstrom J. A., York D. G., 2014, ApJ, 792, 106
- Whittet D. C. B., Martin P. G., Hough J. H., Rouse M. F., Bailey J. A., Axon D. J., 1992, ApJ, 386, 562
- Wilking B. A., Lebofsky M. J., Kemp J. C., Martin P. G., Rieke G. H., 1980, ApJ, 235, 905
- Zubko V., Dwek E., Arendt R. G., 2004, ApJS, 152, 211